Molecular Vision 2024; 30:37-48 <http://www.molvis.org/molvis/v30/37>
Received 20 February 2023 | Accepted 10 February 2024 | Published 16 February 2024

The importance of the fourth Greek key motif of human γD-crystallin in maintaining lens transparency—the tale told by the tail

Venkata Pulla Rao Vendra,[1] Madhupreetha Thangapandian[2]

[1]Ophthalmic Molecular Genetics Section, Ophthalmic Genetics and Visual Function Branch, National Eye Institute, National Institutes of Health, Bethesda, MD; [2]Department of Biotechnology, K.S.Rangasamy College of Technology, Tamil Nadu, India

Purpose: Congenital cataract affects 1–15 per 10,000 newborns worldwide, and 20,000–40,000 children are born every year with developmental bilateral cataracts. Mutations in the crystallin genes are known to cause congenital cataracts. Crystallins, proteins present in the eye lens, are made up of four Greek key motifs separated into two domains. Greek key motifs play an important role in compact folding to provide the necessary refractive index and transparency. The present study was designed to understand the importance of the fourth Greek key motif in maintaining lens transparency by choosing a naturally reported Y134X mutant human γD- crystallin in a Danish infant and its relationship to lens opacification and cataract.

Methods: Human γD-crystallin complementary DNA (cDNA) was cloned into the pET-21a vector, and the Y134X mutant clone was generated by site-directed mutagenesis. Wild-type and mutant proteins were overexpressed in the BL21 DE3 pLysS cells of *E. coli*. Wild-type protein was purified from the soluble fraction using the ion exchange and gel filtration chromatography methods. Mutant protein was predominantly found in insoluble fraction and purified from inclusion bodies. The structure, stability, aggregational, and amyloid fibril formation properties of the mutant were compared to those of the wild type using the fluorescence and circular dichroism spectroscopy methods.

Results: Loss of the fourth Greek key motif in human γD-crystallin affects the backbone conformation, alters the tryptophan micro-environment, and exposes a nonpolar hydrophobic core to the surface. Mutant is less stable and opens its Greek key motifs earlier with a concentration midpoint (C_M) of unfolding curve of 1.5 M compared to the wild type human γD-crystallin (C_M: 2.5 M). Mutant is capable of forming self-aggregates immediately in response to heating at 48.6 °C.

Conclusions: Loss of 39 amino acids in the fourth Greek key motif of human γD-crystallin affects the secondary and tertiary structures and exposes the hydrophobic residues to the solvent. These changes make the molecule less stable, resulting in the formation of light-scattering particles, which explains the importance of the fourth Greek key in the underlying mechanism of opacification and cataract.

Blindness is one of the most significant disabilities in the developing world. According to the World Health Organization (WHO) estimates of 2004, nearly 37 million people around the world were blind, including 1.36 million children. Cataract is one of the major causes of blindness, accounting for 47.8%, followed by glaucoma (12.3%), age-related macular degeneration (8.7%), and diabetic retinopathy (4.8%) [1]. The occurrence of congenital cataract in the most underdeveloped regions of the world is 5 to 15 per 10,000 children [2]; every year, 20,000 to 40,000 children are born with developmental bilateral cataracts [3].

Cataract is commonly referred to as protein condensation disease, which causes opacification of the eye lens. Protein condensation diseases develop from the loss of protein solubility, which leads to the formation of a condensed phase, such as a dense liquid or solid phase, a gel phase, a distribution of globular protein aggregates, or a distribution of protein fibrils of varied lengths [4]. Pathological studies of cataractous lenses reveal that cataracts are composed of protein aggregates that precipitate in eye lens cells [5]. Insoluble proteins obstruct the passage of light through the lens, thereby blocking light from reaching photoreceptor cells in the retina.

Crystallins are the most abundant proteins present in the vertebrate eye lens. Crystallins comprise 90% of the total lens protein content, and their higher concentrations and short-range spatial order provide the necessary refractive index and transparency to the eye lens [6,7]. Greek key motifs in crystallins produce much greater refractive increments, more salt bridges, and particular amino acid substitutions, such as lysine and glutamic acid residues are switched out for arginine and aspartic acid, respectively, causing the refractive increment to rise [8]. Additionally, structural elements such as hydration, short-range interactions, and π-π interactions

Correspondence to: Venkata Pulla Rao Vendra, OMGS/OGVFB/NEI/NIH, 5625 Fishers Ln, Room 1S24, Rockville, MD 20852; Phone: (301) 594-7055. email: pullaraovv@gmail.com, venkatapullarao.vendra@nih.gov.in

affect the protein refractive index [9]. Crystallins, which are highly stable and water-soluble, are classified into three major subgroups based on their molecular weights (α, β, and γ). The transparency of the eye lens is primarily caused by the regular arrangement of crystallins in lens fiber cells. The following crystallins are developmentally expressed in mammalian lens tissue: αA, αB, βB1, βB2, βB3, βA1/A3, βA2, βA4, γA, γB, γC, γD, γE, γF, and γS [10,11]. Among the γ-crystallins, γC and γD-crystallins are enriched in the lens nucleus [12].

Human γD crystallin is a β-sheet rich, 174 amino acid (initial methionine is counted), two domain protein. Each domain is made up of two Greek keys, and each Greek key comprises four β-pleated sheets that are arranged in an antiparallel pattern. Each linear four-stranded motif in the double Greek key motif domain exchanges its third β-strand for the first β-sheet that belongs to its partner motif, giving the domain a complex topology [13]. Greek key motif 1 spans residues 1–40, motif 2 covers sequence 42–83, motif 3 is in the residues between 88 and 128, and the final Greek key is in the stretch of 129–171 [14]. The N-terminal domain of γD-crystallin is less stable than the C-terminal and full-length proteins [15]. In contrast, the isolated N-terminal domain is more stable than the C-terminal domain in βA3-crystallin and γS-crystallin [15,16].

A nonsense mutation in the human γD-crystallin gene at the c.418C>A nucleotide level is reported in a Danish infant, leading to the premature stop codon at the 134th position, causing loss of the last 39 amino acids of the protein and associated with congenital cataract microcornea (CCMC) [17]. This truncated protein may lead to cataract by acting in a dominant–negative manner; the exact mechanisms by which protein abnormalities result in a decrease in lens transparency are currently unknown. The present study was designed to understand the structural basis of a Y134X mutant human γD-crystallin molecule associated with congenital cataract. In addition, further evidence for the importance of the fourth Greek key motif to the structural properties of human γD-crystallin and the maintenance of lens transparency was provided. An in-depth structural analysis of the mutant protein in vitro in aqueous solution is presented, in which the Y134X mutant was compared with that of the wild-type molecule. The loss of the last 39 residues in the C-terminal domain of human γD-crystallin affects the fourth Greek key motif, altering the structure, stability, and aggregation properties and resulting in the formation of light-scattering particles, potentially leading to cataract.

METHODS

Cloning and site-directed mutagenesis: Wild-type cDNA (NM_006891.3) was cloned into the pET-21a vector, as described earlier [18]. The Y134X mutant clone was generated by site-directed mutagenesis using the following primers: forward 5′ CTG GGT CCT CTA AGA GCT GTC CAA CTA CCG AGG ACG G 3′ and reverse 5′ GTA GTT GGA CAG CTC TTA GAG GAC CCA GGA GCC CTC C 3′. Methylated wild-type DNA was cleaved into fragments by the *DpnI* restriction enzyme, and the remaining intact plasmid with the desired mutation was transformed into *E. coli* DH5α cells. Plasmids were isolated and sequenced for the respective changes using a genetic analyzer (ABI 3130; Thermo Fisher Scientific, Waltham, MA).

Overexpression of recombinant proteins: The recombinant constructs pET21-a-γD and pET21-a-γD-Y134X were transformed into *E. coli* BL21 (DE3) pLysS cells. A single colony containing the pET21-a-recombinant plasmid was picked and inoculated into 15 ml of Luria-Bertani (LB) medium containing 50 µg/ml ampicillin and 34 µg/ml chloramphenicol. It was then grown for 12 h by shaking at 225 rpm at 37 °C. Ten mL of this grown culture was then transferred into 1 liter of the above medium with the same concentration of antibiotics. The cultures were grown at 37 °C to an absorbance value of 0.6–0.8 at 600 nm. Recombinant protein synthesis was induced by the addition of isopropyl-β-D thiogalactopyranoside (IPTG) at a final concentration of 1 mM at 37 °C, and the culture was grown for an additional 3.5 h. Cells were pelleted down from the 1 liter culture by centrifugation at 6000 ×g for 10 min at 4 °C.

The pellets were suspended in 40 ml of lysis buffer containing 50 mM Tris-Cl (pH 7.3), 150 mM NaCl, 5 mM dithiothreitol (DTT), 100 mM phenyl methyl sulfonyl fluoride (PMSF), and 1 mM ethylenediaminetetraacetic acid (EDTA). The cell suspension was extensively sonicated for 16 cycles, each cycle comprising 30 s pulse on at 35% amplitude and 30 s pulse off at 4 °C using a high-intensity ultrasonic processor (Sonics Vibra Cell; Sonics and Materials Inc., Newton, MA). The cell lysate was centrifuged at 30,000 ×g for 20 min at 4 °C. The supernatant and pellet were checked for the presence of the protein on 14% sodium dodecyl sulfate polyacrylamide gel electrophoresis (SDS-PAGE). The wild-type protein was found in the soluble fraction, and the Y134X mutant was predominantly found in the insoluble fraction; therefore, the insoluble fraction was chosen as a source to purify the mutant protein.

Purification of the wild-type and Y134X mutant proteins: The wild-type human γD-crystallin protein was purified as described earlier [19]. The mutant was purified from the

insoluble pellet. The insoluble pellet was resuspended in 9 ml of washing buffer-1 (25 mM Tris-Cl (pH 8.0), 100 mM KCl, 0.1% Triton X 100, 1.5 M urea, and 2 mM DTT) and washed 4 times by centrifugation at 30,000 g for 20 min at 4 °C until a clear supernatant was obtained. The pellet was then washed with buffer lacking urea and Triton X 100 (buffer-2), dissolved in the buffer containing 50 mM Tris (pH 7.3) and 8 M urea (buffer 3), and stirred continuously to solubilize the protein at 4°C for 12 h. The urea was removed slowly using the stepwise dialysis method. The purity of the protein was assessed by SDS–PAGE (Appendix 1). The concentration of the protein was measured by absorbance at 280 nm and calculated by its molar extinction coefficient.

Structural analysis: The secondary structures of the wild-type and Y134X mutant proteins were analyzed far-ultraviolet circular dichroism (far-UV CD) spectra in the 250–190 nm range. The protein concentration used to determine the far-UV CD spectra was 0.1 mg/ml in 10 mM Na_2HPO_4/NaH_2PO_4 (pH 7.3). Spectra were recorded with 2 mm path-length quartz cells at 100 nm/min speed using a dichrograph instrument (J-810; Jasco, Easton, MD) at room temperature (27 °C). At least three independent runs of three separate samples were measured and averaged, and the blank values of the corresponding buffer were subtracted from those of each protein. Ellipticity was normalized and presented.

The tertiary structure was assessed with tryptophan emission fluorescence. The spectra were recorded using a fluorescence spectrophotometer (F-2500; Hitachi, Yokohama, Japan) in the range of 305–400 nm using an excitation wavelength of 295 nm, with 5 nm excitation and emission slits. The protein concentration used for determining the tryptophan emission fluorescence spectra was 6 µM in 50 mM Tris-Cl (pH 7.3), 150 mM NaCl, 5 mM DTT, and 1 mM EDTA.

Quenching experiments were performed using potassium iodide (KI) as a surface quencher. Protein samples of 15 µM in 50 mM Tris-Cl (pH 7.3), 150 mM NaCl, 5 mM DTT, and 1 mM EDTA were incubated with 0–1 M KI in the dark for 15 min, and the spectra were recorded between 310 and 400 nm by exciting at 295 nm. Excitation and emission slits were kept at 10 nm, while the spectra were recorded. The results were analyzed using the Stern–Volmer approach [20].

Extrinsic fluorescence spectra of proteins were recorded using probes, namely 4,4- dianilino-1,1- binaphthyl-5,5-disulfonate (bis-ANS), 8-anilino-1-naphthalene-sulfonate (ANS), and 9-diethylamino- 5H-benzo[alpha]phenoxazin-5-one (Nile red). Protein samples of 6 µM in 50 mM Tris-Cl (pH 7.3), 150 mM NaCl, 5 mM DTT, and 1 mM EDTA were incubated with 0–120 µM of bis-ANS or Nile red or 0–160 µM of ANS in the dark for 30 min, and spectra were recorded between 400–600 nm with bis-ANS and ANS, and 570–700 nm for Nile red by exciting at 390 and 540 nm, respectively. The excitation and emission slits for bis-ANS were 2.5 nm, for ANS 5 nm, and for Nile red 10 nm.

Stability: Equilibrium unfolding experiments using guanidium hydrochloride (GuHCl) were conducted to check the stability of the mutant protein. Purified proteins were diluted to 0.1 mg/ml in a series of solutions ranging from 0 to 4.5 M GuHCl with 0.1 increments in a buffer containing 50 mM Tris, 150 mM NaCl, 1 mM EDTA, and 5 mM DTT. Protein samples were incubated at 37 °C for 24 h. Fluorescence emission spectra were recorded in the range of 310 to 400 nm using an excitation wavelength of 295 nm, with 10 nm excitation and emission slits. The values of ΔG° were calculated using the following Equation [21]:

$$\Delta G^\circ = -RT\ln K$$

Aggregational properties: The formation of amyloid-type fibrils was monitored at room temperature (27 °C) using a 2-[4-(Dimethylamino)phenyl]-3,6-dimethyl-1,3-benzothiazol-3-ium chloride (Thioflavin-T) probe. Protein samples of 9 µM in 50 mM Tris, 150 mM NaCl, and 1 mM EDTA was incubated with 20 µM of Thioflavin-T for 30 min in the dark and excited at a 444 nm wavelength light. The spectra were recorded in the range of 465 nm to 570 nm with 10 nm excitation and emission slits. To find the optimum concentration of Thioflavin-T, 6 µM protein samples in 50 mM Tris, 150 mM NaCl, 1 mM EDTA, and 5 mM DTT were incubated with 0–120 µM of dye in the dark for 30 min, and the spectra were recorded using the same parameters as above. The amyloid fibril formation was further confirmed using Congo red dye and a ultraviolet visible (UV-VIS) spectrophotometer. The same protein concentration and buffer strength used in recording the Thioflavin-T assay were maintained, and the absorption spectra were recorded in the range of 450–600 nm using 1 µM Congo red dye. These two assays were performed at buffers of different pH levels 3, 4, 5, 7.3, 9, and 11.

Thermal aggregation: Time-dependent light scattering was measured for both the wild-type and mutant proteins by heating the 3 µM protein samples in 50 mM Tris-Cl, and 150 mM NaCl at 48.6 °C. Light scattering was measured for 900 s at 600 nm with 2.5 nm slits using a spectrofluorometer. The amount of 300 µl of the heated samples were incubated in the dark for 30 min with 160 µM of ANS, and spectra were recorded using the above-mentioned parameters and settings.

All fluorescence studies were measured three times with three separate samples. These were averaged, and the corresponding buffers were subtracted for each protein.

RESULTS

Mutation alters secondary and tertiary structures: Backbone conformation was assessed using the far-UV CD spectra. Spectra were not identical, and a significant change was observed in the β-sheet (218 nm) and α-helix (206 nm) conformation of the mutant compared to the wild type (Figure 1A). CDPro analysis further confirmed that mutant α-helical content was increased by 4.4%, and the β-sheet component was decreased by 5.5% compared to the wild type, indicating that the secondary structure is altered significantly (Table 1).

The tertiary structure was analyzed using the tryptophan emission fluorescence spectra. Mutant showed an emission maximum of 336 nm, and the wild type exhibited an emission maximum at 326.5 nm (Figure 1B). This red shift confirms that the tryptophan microenvironment in the mutant is changed compared to the wild type.

Potassium iodide (KI) was used to check the surface quenching properties of the proteins. The emission intensity of the Y134X mutant protein decreased and was more pronounced in the mutant with the increasing concentration of a surface quencher KI (Appendix 2) compared to the wild type (Appendix 2). The intensity drop was greater in the mutant compared to the wild type. The emission maxima in the wild type were around 325 nm, and for the mutant, they were around 335 nm. The emission max is redshifted 10 nm in the mutant, which is probably due to a change in the tryptophan microenvironment. The Stern–Volmer plot (Figure 1C) shows that the wild-type and mutant Stern–Volmer values (Ksv) are 0.1765 ± 0.013 and 0.6761 ± 0.019, respectively. This demonstrates that mutant tryptophans are quenched more efficiently than the wild type.

Mutant exposes its hydrophobic core: The surface hydrophobicities of the wild type and mutant were measured using bis-ANS, ANS, and Nile red dyes. The extrinsic fluorescence of the mutant upon binding to bis-ANS was 13-fold higher at 120 µM of bis-ANS dye compared to the wild type, suggesting a higher degree of surface hydrophobicity in the mutant protein (Figure 2A). ANS was also used, and it was found that the mutant showed more surface hydrophobicity (Appendix 3). Figure 2B confirms this with another dye, Nile red. The fluorescence intensity is 11 times higher in the mutant compared to the wild type, with Nile red dye at 120 µM declaring that the mutant has a higher self-aggregating propensity.

Mutant is less stable: GuHCl, a chemical denaturant, was used to study the stability of the mutant and wild-type molecules. Figure 3 shows the unfolding curves of the wild type and Y134X mutant. The fluorescence intensity ratio 350/330 was plotted against the GuHCl concentration. Both the wild-type and mutant proteins exhibited two-state transitions with single intermediates. The wild type displayed an unfolding transition around 1.6–3.6 M GuHCl, but for the mutant, it lay between 0.6–3.2 M GuHCl. The transition midpoints (C_M) for the wild-type and mutant unfolding curves were 2.5 and 1.5 M, respectively. The ΔG values were calculated from the unfolding curves and are presented in Appendix 4. The Y134X mutant and wild-type ΔG plots crossed the zero line at 1.55 M and 2.6 M GuHCl concentration. The ΔG° values calculated from the unfolding curves for the wild type and the mutant were 7.56 K.cal.mol^{-1} and 2.375 K.cal.mol^{-1}, respectively (Table 2). These results prove that the mutant is less stable compared to the wild type. The residuals deviating from fitted line were within the limits, confirming that the two-state fitting was appropriate for the unfolding curves (Appendix 4).

Mutant is not capable of forming amyloid fibrils: The formation of amyloid fibrils was checked by incubating the protein samples with Thioflavin-T at acidic, physiologic, and basic pH levels. The protein samples were incubated with 0–120 µM of Thioflavin-T to determine the appropriate concentration of the dye. It was found that 20 µM dye is optimal for the spectra, and the same concentration was maintained in further experiments (Appendix 5). The mutant emitted a fluorescence intensity that was 9.6 times higher at pH 7.3 and at emission maxima compared to the wild type when 20 µM of Thioflavin-T was bound (Figure 4A). To ensure these were amyloid fibrils, a kinetic assay was performed and found a little decrease in the fluorescence after 72 h for the mutant and a slight increase in the fluorescence for the wild type. (Figure 4B). The Thioflavin-T fluorescence emission intensities were more pronounced in the mutant protein at pH 9 and 11 at emission maxima when 20 µM of Thioflavin-T was bound, whereas they were less pronounced in the wild type. The emission intensity was increased about six to eightfold (i.e., 8.4 and 6.5 at pH 9 and 11, respectively) in the mutant compared to the wild type (Appendix 6). The Thioflavin-T fluorescence in the mutant at acidic pH 3, 4, and 5 was only about 2.1-, 1.5-, and 1.8-fold, respectively, compared to the wild type (Appendix 6). The amyloid fibril formation was further checked with the absorbance spectra in the wavelength range of 450–600 nm by Congo red. The absorbance maximum of the mutant was slightly red-shifted at pH 7.3 and blue-shifted at pH 9 and 11, whereas these shifts were not prominent in the case of the wild type with Congo red dye (Appendix 7). These two assays confirm that the mutant did not form amyloid fibrils.

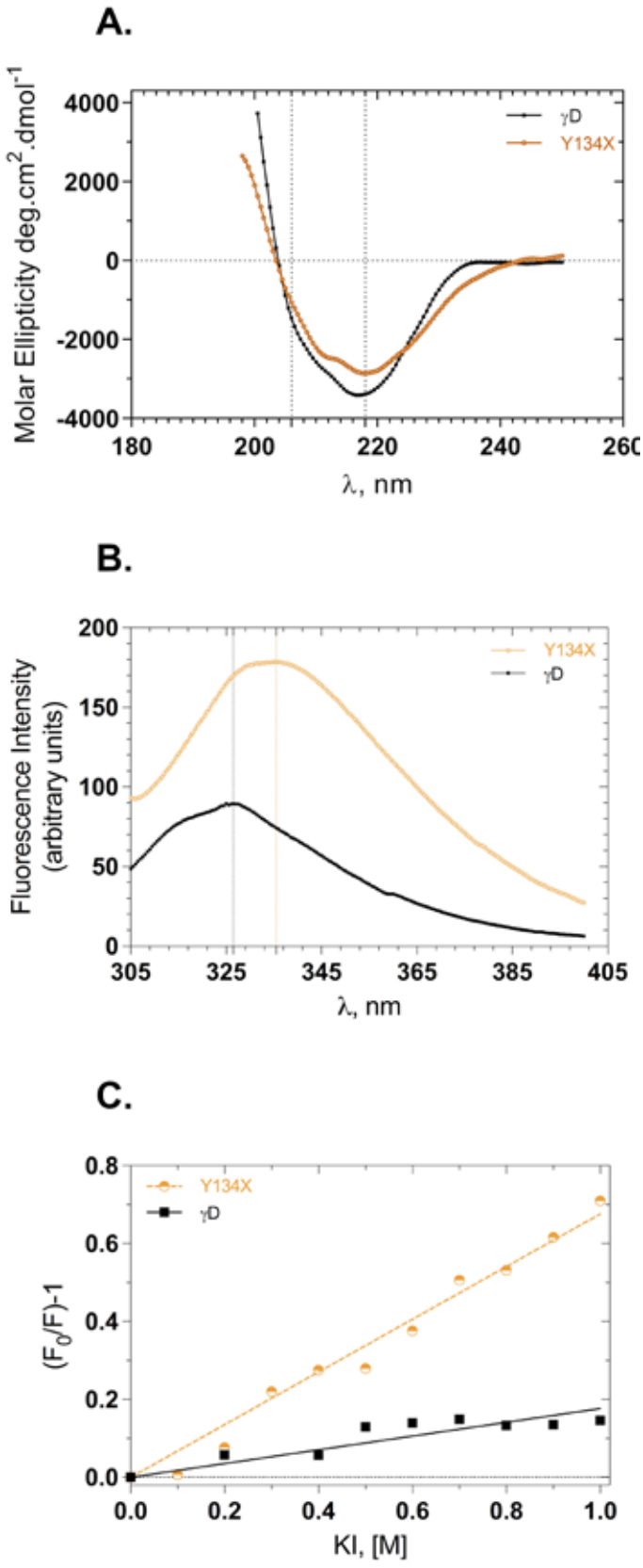

Figure 1. Structural properties of wild-type (black squares) and Y134X mutant human γD- crystallin (brown circles). **A**: Far-ultraviolet circular dichroism spectra. Protein concentration: 0.1 mg/ml; cell path length: 2 mm; scanning speed: 100 nm/min. Vertical lines at 218, and 206 nm represent β-sheet and α-helix conformations respectively. Each spectrum is an average of three independent scans of three separate samples. **B**: Intrinsic fluorescence spectra. Protein concentration: 6 µM; λ_{ex}: 295 nm; excitation emission slits: 5 nm. Vertical lines represent the emission maxima of the proteins. Each spectrum is an average of three independent scans of three separate samples. **C**: Stern–Volmer plots. Protein concentration: 15 µM; λ_{ex}: 295 nm; excitation emission slits: 10 nm. The line indicates the fitted data, and the blocks stand for raw data. F_0: fluorescence intensity of the protein; **F**: fluorescence intensity of the protein in the presence of a quencher. The data were acquired from three independent runs of three separate samples.

Table 1. Deconvoluted CD spectra of wild-type and Y134X mutant human γD-crystallin.

Protein	% Helix (r)	% Helix (d)	% Helix (total)	% β-Sheet (r)	% β-Sheet (d)	% β-Sheet (total)	% turn	% unordered
γD	1.7	6.5	8.2	31.6	21	52.6	22.8	15.6
γD-Y134X	2.5	10.1	12.6	24.1	23	47.1	21.4	19.3

Abbreviations: r: regular; d: denatured

Mutant self-aggregates at high temperatures: The light-scattering properties of the wild-type and mutant proteins were evaluated by heating the proteins at 48.6°C for 900 s. The wild type did not scatter the light throughout the san, but the mutant started to show the light scattering particles immediately and reached a maximum of around 800 s, demonstrating that the mutant is prone to aggregation at elevated temperatures (Figure 5). The heated samples were further analyzed with the surface hydrophobicity-detecting dye ANS, and it was found that the heated Y134X mutant showed 1.7 times more fluorescence with ANS compared to the unheated samples (Appendix 8).

DISCUSSION

Three truncated proteins (Y134X, R140X, and W157X) and one frameshift mutation (G165fs) have been reported so far in the human γD-crystallin protein, affecting the fourth Greek key motif; they are associated with congenital cataracts. In the mutant R140X, the deleted region contains three β-strands corresponding to the two Greek key motifs that are essential components of the C-terminal domain's jellyroll fold. The loss of three β-strands in the fourth Greek key motif disturbs interdomain interactions and results in the loss of secondary and tertiary structures and a decrease in stability. Greater access of polar and nonpolar residues to the surface is expected to result in molecule aggregation [19]. In the other C-terminal truncated mutant W157X and frame shift mutant G165fs, the last β-stand (166–170) corresponds to the fourth Greek key motif that is lost or broken and leads to a situation quite similar to R140X. The loss of the penultimate and last β-strand in the W157X mutant affects the tertiary structure and surface hydrophobicity, leading to weakening of the molecule and forming homo aggregates at higher temperatures [18]. G220X is one such nonsense mutation reported

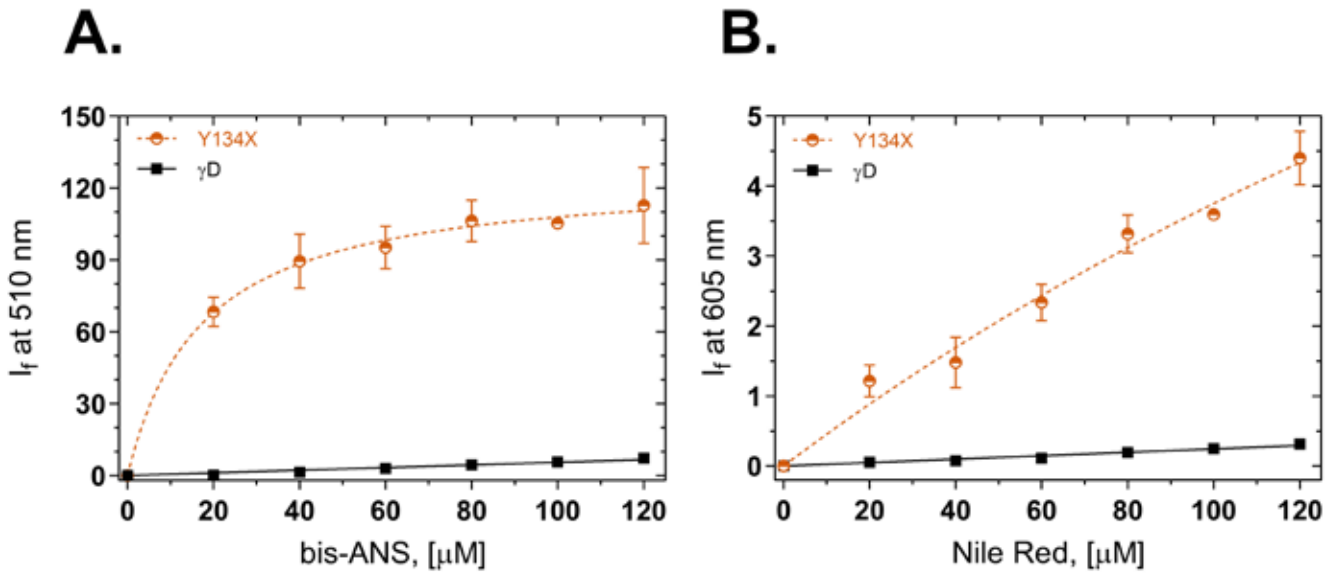

Figure 2. Surface hydrophobicity measurement of wild-type (black squares) and Y134X mutant human γD-crystallin (brown circles). **A**: bis-ANS spectra. Values represent the mean of three independent experiments; error bars indicate the standard deviation. Protein concentration: 6 μM; λ_{ex}: 390 nm; λ_{em}: 510 nm; excitation emission slits: 2.5 nm. **B**: Nile red spectra. The data are the average of three independent experiments of three separate samples. Error bars indicate the standard deviation. Protein concentration: 6 μM; λ_{ex}: 540 nm; λ_{em}: 605 nm; excitation emission slits: 10 nm. I_f: fluorescence intensity.

Table 2. Thermodynamic values calculated from the GuHCl unfolding curves shown in Figure 3.

Protein	C_M [a]	ΔG⁰ [b]	m [c]	R^2	P value
γD-WT (UF)	2.546 ± 0.01	7.560 ± 0.206	2.184 ± 0.079	0.9983	<0.0001
γD-Y134X (UF)	1.513 ± 0.03	2.375 ± 0.170	1.569 ± 0.093	0.9863	<0.0001

[a]Midpoint of GuHCl unfolding curve in M;[b] Free energy of unfolding in the absence of GuHCl in (K.cal.mol^{-1}); [c] Slope of GuHCl versus fraction unfolded ratio in (Kcal.mol^{-1}M^{-1}); UF: unfolded. Abbreviations: C_M: Concentration midpoint; GuHCl: Guanidium hydrochloride; RFU: Relative fluorescence units.

in the βB1-crystallin. The mutation G220X is predicted to be a truncated protein, which lacks a partial fourth Greek key and complete c-terminal arm and severely affects solubility, resulting in autosomal dominant bilateral pulverulent congenital cataract [22].

In the present study, the change of tyrosine to stop codon at the 134th position leads to a truncated protein and causes a change in the structure, stability, and aggregational properties. γD-crystallin shows prominent bands at 218 and 206 nm, which stand for β-sheet and α-helix conformation in the far-UV CD spectra. The wild type displayed distinguished bands at 218 and 206 nm, which align with the published results [15]. The mutant's ellipticity at 218 nm was -2857 units, while the wild type had -3384 units. The decrease was -527 units; this could be due to the loss of the fourth Greek key motif's β-sheets due to truncation. CDPro analysis of secondary structures was performed with the CDSSTR program, with the SMP50 protein data set as a reference [23]. The wild type showed a β-sheet and α-helical contents of 52.6% and 8.2%, respectively, which is in close agreement with the published results [15]. The mutant exhibited a 4.4% higher proportion of α-helices and a 5.5% lower amount of β-sheets, indicating the secondary structure is significantly altered in the mutant due to the loss of 39 amino acids.

Four tryptophans at positions 43, 69, 131, and 157 are present in human γD-crystallin. Of the four tryptophans, two are well buried (W43 and W131), and the other two are exposed to the surface (W69 and W157) to some extent [24]. This property was taken into consideration, and the tertiary structure and tryptophan microenvironment were evaluated. The wild type showed an emission maximum of 326.5 nm, which aligns with earlier reports [15]. The tryptophan emission fluorescence was two fold higher at emission maximum and 9.5 nm red-shifted in the mutant, confirming that the

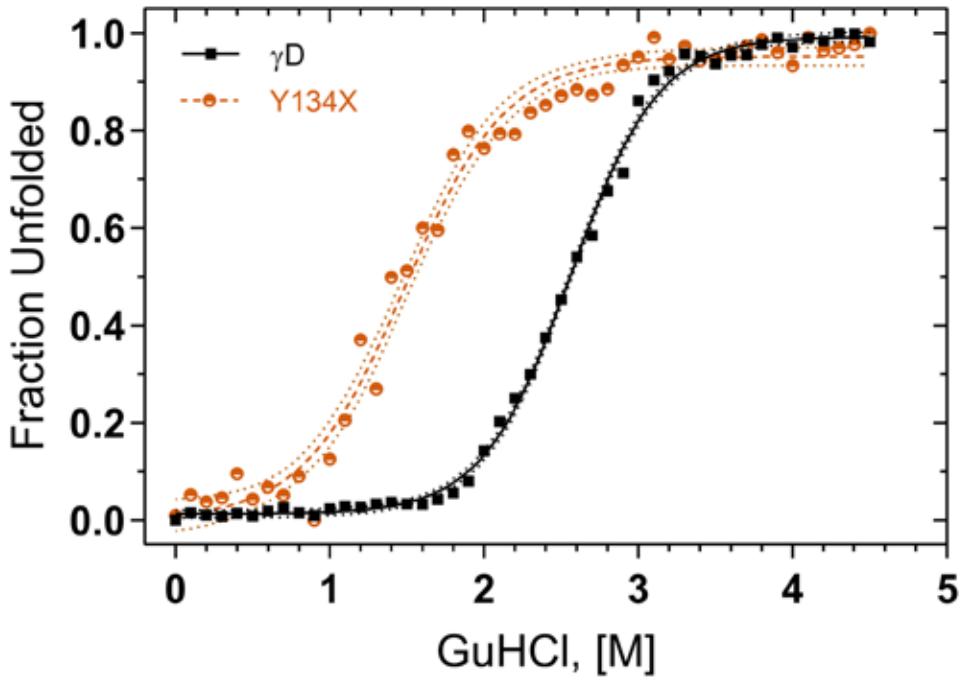

Figure 3. Guanidine hydrochloride unfolding of wild-type (black squares) and Y134X mutant human γD-crystallin (brown circles). Protein samples were excited at 295 nm, and the relative emission intensity of the 350 nm fluorescence (denatured form) was compared to that of the 330 nm (native protein) and recorded as a function of the denaturant concentration. The line indicates the fitted data, and the blocks stand for raw data. Protein concentration: 0.1 mg/ml; excitation emission slits: 10 nm. The data were acquired from two independent experiments of two separate sets of samples.

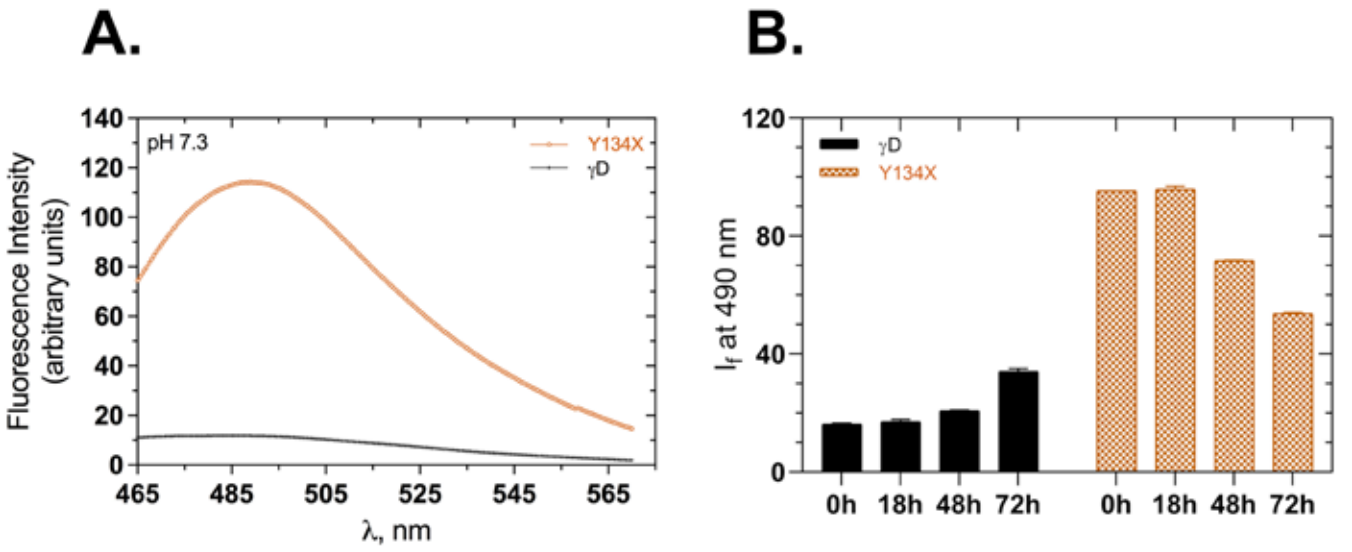

Figure 4. Amyloid fibril detection of wild-type (black +) and Y134X mutant human γD-crystallin (brown circles) using Thioflavin-T. **A**: Thioflavin-T spectra at pH 7.3. Each spectrum is an average of three independent scans of three separate samples. **B**: Thioflavin-T fluorescence at pH 7.3 as a function of time. Values represent the mean of three independent experiments of three separate samples; error bars indicate the standard deviation. Protein concentration: 9 µM; λ_{ex}: 444 nm; excitation and emission slits: 10 nm. I_f: Intensity of fluorescence.

microenvironment around the tryptophans is significantly altered. The mutant Y134X displayed an emission maximum of 336 nm. This is in agreement with the other mutants, R140X, W157X, and G165fs, affecting the fourth Greek key motif, which show their emission maxima at 337, 336, and 337 nm, respectively [18,19]. This further confirms that aromatic side chains in these mutants affecting the fourth

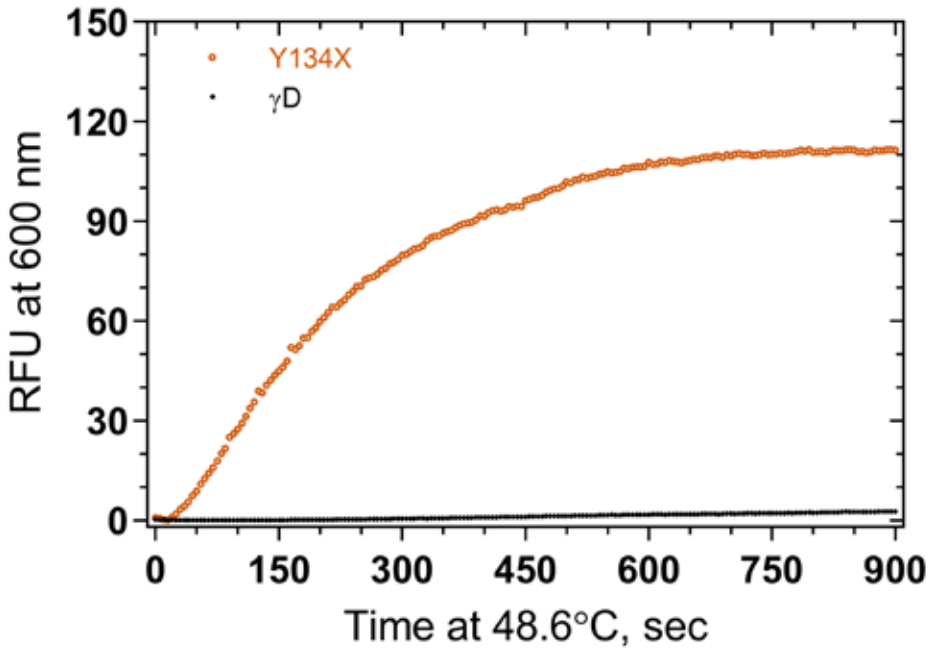

Figure 5. Time-dependent light scattering of wild-type (black diamonds) and Y134X mutant human γD-crystallin (brown circles) at 48.6 °C. The data were acquired from three independent runs of three separate samples. Protein concentration: 3 µM; λ_{ex}: 600 nm; λ_{em}: 600 nm; excitation and emission slits: 2.5 nm. RFU: relative fluorescence units.

Greek key motif are somewhat more exposed to the surface of the protein.

KI was used to study the surface quenching of the proteins [20]. Mutant fluorescence intensity did decrease and was more pronounced at emission maximum in the 0–1 M KI range, whereas the wild-type intensity did decrease and become less pronounced when KI was used as a surface quencher. The greater accessibility of a surface quencher molecule to the exposed tryptophan residues in the protein could be the cause of the decrease in emission intensity. The wild type exhibited emission maxima around 325 nm, and for the mutant, they were around 335 nm. The mutant showed 10 nm red shift with KI when compared to the wild type. Wild-type tryptophans in this study were buried and not exposed to water (class 1), and mutant tryptophans were edge-exposed (class 2) [25]. This classification is based on the assumption that tryptophan residues play a crucial role in protein stability and function. Class 1 tryptophans are typically found in the hydrophobic core of proteins shielded from the aqueous environment, while class 2 tryptophans are located at the protein surface, potentially interacting with solvent molecules or other proteins. The KI quenching Ksv values of the wild type and the mutant were 0.1765 ± 0.013 and 0.6761 ± 0.019, respectively. This demonstrates that tryptophans are quenched more in the mutant than in the wild type.

Bis-ANS is a negatively charged dye that has the ability to bind to the hydrophobic patches present on the surface of the protein and emit a fluorescence signal around 510 nm when excited at 390 nm [26]. Nile red is a neutral dye that detects the tendency of a protein to self-aggregate when excited at 540 nm [27]. Mutant Y134X exhibited a greater amount of fluorescence with both dyes compared to the wild type; this is in agreement with the other mutants R140X, W157X, and G165fs affecting the fourth Greek key motif [18,19]. The extrinsic fluorescence analysis of the mutant Y134X using two probes reveal that the exposure of hydrophobic residues to the surface of the protein.

Highly conserved tryptophans are present in each domain of the human γD-crystallin. The unfolding and refolding progression of the protein was studied with the help of these tryptophans using fluorescence spectroscopy [28]. The denatured protein exhibits higher fluorescence and red-shifted compared to the native state due to tryptophan fluorescence quenching in the native state [29]. The ΔC_M and ΔΔG for the mutant were 1.033 M and 5.185 K.cal.mol^{-1}, respectively. The other mutant, R140X, which is seen to disturb the fourth Greek key motif, shows ΔC_M and ΔΔG values of 0.98 M and 5.11 Kcal.mol^{-1}, respectively; this is in close agreement with the current study [19]. This states that the stability of the mutant to the GuHCl was found to be lower compared to the wild type.

The isolated N-terminal domain of γD-crystallin is less stable than the C-terminal domain, as well as the full-length protein. This difference in stability suggests that the interdomain interface contributes ΔG_{H2O} of 4.2 K.cal.mol^{-1} and plays a crucial role in maintaining the overall structural integrity of γD-crystallin [15,30]. The isolated γD-crystallin N-terminal domain destabilizes with a C_M of 1.2 M GuHCl, while the C-terminal region displays a C_M of 2.7 M GuHCl. The γS-WT exhibits a C_M value of 2.3 M GuHCl, while equilibrium unfolding experiments of the individual γS-N and γS-C-terminal domains yield C_M values of 1.7 M and 2.3 M GuHCl, respectively [15,30]. In contrast, the isolated N-terminal domain is more stable than the C-terminal domain in βA3-crystallin and γS-crystallin [15,16]. In the current study, mutant Y134X displayed a C_M of 1.51 M. This finding is consistent with a previous study that shows the importance of the N-terminal domain in maintaining proper protein folding [30]. Additionally, the high C_M value indicates that mutant Y134X may have a stable structure compared to the isolated human γD-N-terminal domain.

Thioflavin-T is a benzothiazole dye commonly used to identify amyloid fibrils, both ex vivo and in vitro [31]. It shows enhanced fluorescence upon binding to amyloid fibrils and is typically used to monitor amyloid fibrils by fluorescence assay [32]. When 20 µM Thioflavin-T was bound, the mutant protein's Thioflavin-T fluorescence emission intensity at basic pHs was 6–8 times higher than that of the wild type, as previously reported in the mutants G61C, R140X, and G165fs of γD-crystallin and the V42M mutant of human γS-crystallin [19,33,34]. This significant increase in fluorescence intensity suggests that the mutant has a higher binding affinity for Thioflavin-T at a basic pH. The kinetic assay with Thioflavin-T did not follow the lag, log, and stationary phases, and significant shifts were not seen in Congo red spectra, as observed in the previous study [35]. This result suggests that the mutant is indeed not capable of forming amyloid fibrils. In the Thioflavin-T kinetic assay, the mutant showed a small decrease in fluorescence after 72 h; a slight increase in fluorescence was seen with the wild type. Alternatively, the decrease in fluorescence in the mutant could be attributed to potential precipitation of the protein due to its weak stability over time, leading to a loss of the fluorescence signal. On the other hand, the slight increase in wild-type fluorescence could be an experimental variation or might suggest an enhanced binding affinity between the altered protein and its fluorophore. However, Thioflavin-T binds to extended β-sheet structures, the affinity of which

varies based on the individual protein and its surface chemistry. The fluorescent intensity observed in this study is probably from the fully or partially opened β-sheets of Greek key motifs 3 and 4.

The formation of light scattering particles is observed in cataracts. Aggregation occurred with the mutant protein immediately when placed at 48.6 °C, while the wild-type protein was scatter-free for 900 s. The mutant W157X also shows light scattering particles readily at 65 °C, which is quite similar to the observation found in this study [18]. This further illustrates that mutant Y134X is more prone to aggregation at elevated temperatures. The Y134X-heated samples emitted more fluorescence when bound to ANS. This increase in fluorescence suggests that the Y134X mutation may have altered the surface hydrophobicity of the protein upon heating, leading to a higher affinity for ANS binding. The enhanced binding affinity for ANS could promote protein–protein interactions, triggering aggregation processes. It is worth remembering that aggregation in γS-crystallin is not directly linked to thermodynamic instability. Local unfolded states, protein dynamics, and hydration also play responsible roles in forming aggregates [36]. The basis for cataract formation is not only the ability of the mutant crystallins to aggregate but rather changes in protein composition and spatial structure that imbalance the lens proteome and alter crystallin interactions [37].

The primary limitation of this study was the need to investigate the relevance of these structural alterations to the lens proteome and α-crystallin interaction; further research is required to understand the implications of these structural changes on the refractive properties of the lens.

Greek key motif 3 covers residues from 88 to 128, while the fourth Greek key motif spans the range from 129 to 171. The mutation Y134X is thought to distort both motifs 3 and 4 since it occurs in the first β-sheet of the fourth Greek key motif and exchanges for the third β-sheet, which is a part of its partner motif (third Greek key motif). This truncation is likely to disrupt the structural integrity of motifs 3 and 4, as it affects the interaction between the two motifs. The distortion caused by the Y134X mutation highlights the intricate relationship between motifs 3 and 4, emphasizing their interdependence in maintaining the overall stability of the protein. Loss of the last 39 residues in the C-terminal domain is seen to affect the third and fourth Greek key motifs, leading to altered structure, stability, and extensive exposure of normally buried nonpolar side chains to the surface, causing self-aggregation. We believe that it is these characteristics that manifest as cataract in the intact lens.

APPENDIX 1.

To access the data, click or select the words "Appendix 1." SDS–PAGE analysis of purified wild-type and Y134X mutant human γD-crystallin proteins. Five µg of protein was loaded and run on 14% SDS–PAGE.

APPENDIX 2.

To access the data, click or select the words "Appendix 2." Fluorescence quenching of wild-type and Y134X mutant human γD-crystallin using KI as a surface quencher. A) Wild-type B) Y134X mutant. Each spectrum is an average of 3 independent scans of 3 separate samples. Protein concentration: 15 µM; λ_{ex}: 295 nm; Excitation emission slits: 10 nm.

APPENDIX 3.

To access the data, click or select the words "Appendix 3." Surface hydrophobicity measurement of wild-type (black squares) and Y134X mutant human γD-crystallin (brown circles) by ANS. Values represent the mean of three independent experiments of 3 separate samples; error bars indicate the standard deviation. Protein concentration: 6 µM; λ_{ex}: 390 nm; λ_{em}: 510 nm; Excitation emission slits: 5 nm. I_f: Fluorescence intensity.

APPENDIX 4.

To access the data, click or select the words "Appendix 4." A) ΔG plots of the GuHCl unfolding curves presented in Figure 3. B) Residual plots of the unfolding curves presented in Figure 3 of wild-type (black squares) and mutant 134X human γD-crystalln (brown circles). The data was acquired from two independent experiments of 2 separate sets of samples.

APPENDIX 5.

To access the data, click or select the words "Appendix 5." Thioflavin-T titration curves of wild-type (black squares) and Y134X mutant human γD-crystallin (brown circles). Each spectrum is an average of 3 independent scans of 3 separate samples. Protein concentration: 6 µM; λ_{ex}: 444 nm; Excitation and emission slits: 5 nm. I_f: Fluorescence intensity.

APPENDIX 6.

To access the data, click or select the words "Appendix 6." Amyloid fibril detection of wild-type (black) and Y134X mutant human γD-crystallin (brown) using Thioflavin-T. Formation of amyloid fibrils at A) pH 9 B) pH 11 C) pH 3 D) pH 4 E) pH 5. Each spectrum is an average of 3 independent scans of 3 separate samples. Protein concentration: 9 µM; λ_{ex}: 444 nm; Excitation and emission slits: 10 nm.

APPENDIX 7.

To access the data, click or select the words "Appendix 7." Congo red absorption spectra of wild-type (black +) and Y134X mutant human γD- crystallin (brown circles). Congo red absorption spectra at A) pH 7.3 B) pH 9 C) pH 11. Each spectrum is an average of 3 independent scans of 3 separate samples. Protein concentration: 9 µM; Cuvette path length: 1 cm.

APPENDIX 8.

To access the data, click or select the words "Appendix 8." Surface hydrophobicity measurement of heated samples of wild-type and Y134X mutant human γD-crystallin by ANS spectra. The data was acquired from three independent experiments of 3 separate samples. Protein concentration: 3 µM; λ_{ex}: 390 nm; Excitation emission slits: 2.5 nm. I_f: Fluorescence intensity.

ACKNOWLEDGMENTS

I thank my mentor Prof. Dorairajan Balasubramanian, Distinguished Scientist and Director Emeritus, Prof. Brien Holden Eye Research Centre, L.V.Prasad Eye Institute, for his valuable guidance, help and support throughout this study. I gratefully acknowledge the ready help and advice of Dr. Rajan Sanakaranarayanan, Mukul JS, Shobha Krupa Rani P, and Pradeep Kumar of the Centre for Cellular and Molecular Biology, Hyderabad, India, and the use of the dichrograph instrument at CCMB. This research was supported by the internal funds of Hyderabad Eye Research Foundation of the L.V.Prasad Eye Institute, Hyderabad.

REFERENCES

1. Resnikoff S, Pascolini D, Etya'ale D, Kocur I, Pararajasegaram R, Pokharel GP, Mariotti SP. Global data on visual impairment in the year 2002. Bull World Health Organ 2004; 82:844-51. [PMID: 15640920].
2. Apple DJ, Ram J, Foster A, Peng Q. Elimination of cataract blindness: a global perspective entering the new millenium. Surv Ophthalmol 2000; 45:Suppl 1S1-196. [PMID: 11291895].
3. Foster A, Gilbert C, Rahi J. Epidemiology of cataract in childhood: a global perspective. J Cataract Refract Surg 1997; 23:Suppl 1601-4. [PMID: 9278811].
4. Benedek GB. Cataract as a protein condensation disease: the Proctor Lecture. Invest Ophthalmol Vis Sci 1997; 38:1911-21. [PMID: 9331254].
5. Aliancy JF, Mamalis N. Crystalline Lens and Cataract. 2017 Aug 15; In: Kolb H, Fernandez E, Nelson R, editors. Webvision: The Organization of the Retina and Visual System [Internet]. Salt Lake City (UT): University of Utah Health Sciences Center.
6. Pierscionek BK, Augusteyn RC. The refractive index and protein distribution in the blue eye trevally lens. J Am Optom Assoc 1995; 66:739-43. [PMID: 8557951].
7. Delaye M, Tardieu A. Short-range order of crystallin proteins accounts for eye lens transparency. Nature 1983; 302:415-7. [PMID: 6835373].
8. Mahendiran K, Elie C, Nebel JC, Ryan A, Pierscionek BK. Primary sequence contribution to the optical function of the eye lens. Sci Rep 2014; 4:5195-[PMID: 24903231].
9. Khago D, Bierma JC, Roskamp KW, Kozlyuk N, Martin RW. Protein refractive index increment is determined by conformation as well as composition. J Phys Condens Matter 2018; 30:435101[PMID: 30280702].
10. Bloemendal H, de Jong W, Jaenicke R, Lubsen NH, Slingsby C, Tardieu A. Ageing and vision: structure, stability and function of lens crystallins. Prog Biophys Mol Biol 2004; 86:407-85. [PMID: 15302206].
11. Lampi KJ, Ma Z, Shih M, Shearer TR, Smith JB, Smith DL, David LL. Sequence analysis of betaA3, betaB3, and betaA4 crystallins completes the identification of the major proteins in young human lens. J Biol Chem 1997; 272:2268-75. [PMID: 8999933].
12. Brakenhoff RH, Aarts HJ, Reek FH, Lubsen NH, Schoenmakers JG. Human gamma-crystallin genes. A gene family on its way to extinction. J Mol Biol 1990; 216:519-32. [PMID: 2258929].
13. Hutchinson EG, Thornton JM. The Greek key motif: extraction, classification and analysis. Protein Eng 1993; 6:233-45. [PMID: 8506258].
14. Basak A, Bateman O, Slingsby C, Pande A, Asherie N, Ogun O, Benedek GB, Pande J. High-resolution X-ray crystal structures of human gammaD crystallin (1.25 A) and the R58H mutant (1.15 A) associated with aculeiform cataract. J Mol Biol 2003; 328:1137-47. [PMID: 12729747].
15. Mills IA, Flaugh SL, Kosinski-Collins MS, King JA. Folding and stability of the isolated Greek key domains of the long-lived human lens proteins gammaD-crystallin and gammaS-crystallin. Protein Sci 2007; 16:2427-44. [PMID: 17905830].
16. Gupta R, Srivastava K, Srivastava OP. Truncation of motifs III and IV in human lens betaA3-crystallin destabilizes the structure. Biochemistry 2006; 45:9964-78. [PMID: 16906755].
17. Hansen L, Yao W, Eiberg H, Kjaer KW, Baggesen K, Hejtmancik JF, Rosenberg T. Genetic heterogeneity in microcornea-cataract: five novel mutations in CRYAA, CRYGD, and GJA8. Invest Ophthalmol Vis Sci 2007; 48:3937-44. [PMID: 17724170].
18. Talla V, Srinivasan N, Balasubramanian D. Visualization of in situ intracellular aggregation of two cataract-associated human gamma-crystallin mutants: lose a tail, lose transparency. Invest Ophthalmol Vis Sci 2008; 49:3483-90. [PMID: 18421082].

19. Vendra VP, Agarwal G, Chandani S, Talla V, Srinivasan N, Balasubramanian D. Structural integrity of the Greek key motif in βγ-crystallins is vital for central eye lens transparency. PLoS One 2013; 8:e70336[PMID: 23936409].

20. Augusteyn RC, Chandrasekher G, Ghiggino KP, Vassett P. Probing the microenvironments of tryptophan residues in the monomeric crystallins of the bovine lens. Biochim Biophys Acta 1994; 1205:89-96. [PMID: 8142489].

21. Pace CN. Determination and analysis of urea and guanidine hydrochloride denaturation curves. Methods Enzymol 1986; 131:266-80. [PMID: 3773761].

22. Mackay DS, Boskovska OB, Knopf HL, Lampi KJ, Shiels A. A nonsense mutation in CRYBB1 associated with autosomal dominant cataract linked to human chromosome 22q. Am J Hum Genet 2002; 71:1216-21. [PMID: 12360425].

23. Sreerama N, Woody RW. On the analysis of membrane protein circular dichroism spectra. Protein Sci 2004; 13:100-12. [PMID: 14691226].

24. Chen J, Flaugh SL, Callis PR, King J. Mechanism of the highly efficient quenching of tryptophan fluorescence in human gammaD-crystallin. Biochemistry 2006; 45:11552-63. [PMID: 16981715].

25. Vivian JT, Callis PR. Mechanisms of tryptophan fluorescence shifts in proteins. Biophys J 2001; 80:2093-109. [PMID: 11325713].

26. Rosen CG, Weber G. Dimer formation from 1-amino-8-naphthalenesulfonate catalyzed by bovine serum albumin. A new fluorescent molecule with exceptional binding properties. Biochemistry 1969; 8:3915-20. [PMID: 5388144].

27. Sutter M, Oliveira S, Sanders NN, Lucas B, van Hoek A, Hink MA, Visser AJ, De Smedt SC, Hennink WE, Jiskoot W. Sensitive spectroscopic detection of large and denatured protein aggregates in solution by use of the fluorescent dye Nile red. J Fluoresc 2007; 17:181-92. [PMID: 17294134].

28. Kosinski-Collins MS, King J. In vitro unfolding, refolding, and polymerization of human gammaD crystallin, a protein involved in cataract formation. Protein Sci 2003; 12:480-90. [PMID: 12592018].

29. Kosinski-Collins MS, Flaugh SL, King J. Probing folding and fluorescence quenching in human gammaD crystallin Greek key domains using triple tryptophan mutant proteins. Protein Sci 2004; 13:2223-35. [PMID: 15273315].

30. Mills-Henry IA, Thol SL, Kosinski-Collins MS, Serebryany E, King JA. Kinetic Stability of Long-Lived Human Lens γ-Crystallins and Their Isolated Double Greek Key Domains. Biophys J 2019; 117:269-80. [PMID: 31266635].

31. LeVine H 3rd. Quantification of beta-sheet amyloid fibril structures with thioflavin T. Methods Enzymol 1999; 309:274-84. [PMID: 10507030].

32. Naiki H, Higuchi K, Hosokawa M, Takeda T. Fluorometric determination of amyloid fibrils in vitro using the fluorescent dye, thioflavin T1. Anal Biochem 1989; 177:244-9. [PMID: 2729542].

33. Zhang W, Cai HC, Li FF, Xi YB, Ma X, Yan YB. The congenital cataract-linked G61C mutation destabilizes γD-crystallin and promotes non-native aggregation. PLoS One 2011; 6:e20564[PMID: 21655238].

34. Vendra VP, Chandani S, Balasubramanian D. The mutation V42M distorts the compact packing of the human gamma-S-crystallin molecule, resulting in congenital cataract. PLoS One 2012; 7:e51401[PMID: 23284690].

35. Papanikolopoulou K, Mills-Henry I, Thol SL, Wang Y, Gross AA, Kirschner DA, Decatur SM, King J. Formation of amyloid fibrils in vitro by human gammaD-crystallin and its isolated domains. Mol Vis 2008; 14:81-9. [PMID: 18253099].

36. Brubaker WD, Freites JA, Golchert KJ, Shapiro RA, Morikis V, Tobias DJ, Martin RW. Separating instability from aggregation propensity in γS-crystallin variants. Biophys J 2011; 100:498-506. [PMID: 21244846].

37. Schmid PWN, Lim NCH, Peters C, Back KC, Bourgeois B, Pirolt F, Richter B, Peschek J, Puk O, Amarie OV, Dalke C, Haslbeck M, Weinkauf S, Madl T, Graw J, Buchner J. Imbalances in the eye lens proteome are linked to cataract formation. Nat Struct Mol Biol 2021; 28:143-51. [PMID: 33432246].

Articles are provided courtesy of Emory University and the Zhongshan Ophthalmic Center, Sun Yat-sen University, P.R. China. The print version of this article was created on 16 February 2024. This reflects all typographical corrections and errata to the article through that date. Details of any changes may be found in the online version of the article.